Earthquakes and Structures, *Vol. 12, No. 6 (2017) 699-712*
DOI: https://doi.org/10.12989/eas.2017.12.6.699

Experimental and analytical evaluation of a low-cost seismic retrofitting method for masonry-infilled non-ductile RC frames

Jarun Srechai[1a], Sutat Leelataviwat[*2], Arnon Wongkaew[1b] and Panitan Lukkunaprasit[3c]

[1]*Department of Civil Engineering, Burapha University, 169 Saen-Sook, Chonburi, 20131, Thailand*
[2]*Department of Civil Engineering, King Mongkut's University of Technology Thonburi,126 Thung Khru, Bangkok, 10140, Thailand*
[3]*Department of Civil Engineering, Chulalongkorn University, 254 Phatumwan, Bangkok, 10330, Thailand*

(Received March 27, 2017, Revised May 20, 2017, Accepted June 20, 2017)

Abstract. This study evaluates the effectiveness of a newly developed retrofitting scheme for masonry-infilled non-ductile RC frames experimentally and by numerical simulation. The technique focuses on modifying the load path and yield mechanism of the infilled frame to enhance the ductility. A vertical gap between the column and the infill panel was strategically introduced so that no shear force is directly transferred to the column. Steel brackets and small vertical steel members were then provided to transfer the interactive forces between the RC frame and the masonry panel. Wire meshes and high-strength mortar were provided in areas with high stress concentration and in the panel to further reduce damage. Cyclic load tests on a large-scale specimen of a single-bay, single-story, masonry-infilled RC frame were carried out. Based on those tests, the retrofitting scheme provided significant improvement, especially in terms of ductility enhancement. All retrofitted specimens clearly exhibited much better performances than those stipulated in building standards for masonry-infilled structures. A macro-scale computer model based on a diagonal-strut concept was also developed for predicting the global behavior of the retrofitted masonry-infilled frames. This proposed model was effectively used to evaluate the global responses of the test specimens with acceptable accuracy, especially in terms of strength, stiffness and damage condition.

Keywords: non-ductile frame; masonry infill; seismic retrofitting; cyclic test; macro model

1. Introduction

Reinforced concrete (RC) frames with un-reinforced masonry (URM) infill panels are commonly used in many areas around the world, especially in low-rise buildings. Earthquake reconnaissance in past earthquakes has observed the poor performance of this structural system, especially when the RC frames are non-ductile (Sezen *et al*. 2003, Kyriakides and Billington 2008). Several failure modes can occur in both the masonry infill panel and surrounding RC frame, depending on the properties of the URM infill panel and the surrounding RC frame (Paulay and Priestly 1992, FEMA 1998, Shing and Mehrabi 2002, Asteris *et al*. 2011). One of the common failure modes included undesirable abrupt shear failure of the bounding columns or beam-column joints due to the transfer of the large strut force from the infill to columns following corner crushing of the panel. This could occur not only in a strong earthquake but also during a moderate shaking, such as the one occurred in Chiangrai, Thailand in 2014 (Lukkunaprasit *et al*. 2016). Model tests as well as full-scale tests have also yielded similar results (Bertero and Brokken 1983, Mehrabi *et al*. 1996, Al-Chaar *et al*. 2002, Lee and Woo 2002, Corte *et al*. 2008, Shing *et al*. 2009). The failure could occur at a relatively small story drift as low as 0.3%. However, if the failure of the bounding elements is prevented, test results as well as actual cases have indicated the beneficial effect of masonry infills in significantly increasing the lateral strength of the frame (Fardis and Panagiotakos 1997, Hassan and Sozen 1997, Mostafaei and Kabeyasawa 2004, Pinto and Taucer 2006, Pujol and Fick 2010, Gómez-Martínez *et al*. 2012). For this reason, several past studies have tried to utilize the infill panels by strengthening them with various materials. Notable strengthening methods include wire-fabric reinforcement, wire-mesh reinforcement, and carbon-fiber-reinforced polymer (CFRP) strip reinforcement. As early as the 1980s, Bertero and Brokken (1983) investigated the effects of masonry and lightweight concrete infill panels on the behavior of RC buildings. Several sub-assemblage models were tested under cyclic or monotonic loads. Both reinforced and un-reinforced masonry infill panels were employed. Experimental results revealed that the effective lateral stiffness increased from 2 to 12 times and the maximum lateral resistance of infilled frames increased from 3 to 8 times compared with those of the bare frames depending upon infill-panel type. It was found that solid brick infills reinforced externally with welded wire and fabric plastered with cement mortar exhibited superior performance to other types of infills.

∗Corresponding author, Associate Professor
E-mail: sutat.lee@kmutt.ac.th
[a]Ph.D.
E-mail: srechai@eng.buu.ac.th
[b]Assistant Professor
E-mail: arnonw@eng.buu.ac.th
[c]Professor Emeritus
E-mail: lpanitan@chula.ac.th

ISSN: 2092-7614 (Print), 2092-7622 (Online)

Buildings with such infills were estimated to be capable of resisting an earthquake with an effective peak ground motion as high as 0.4 g. Other studies (Calvi and Bolognini 2001, Acun and Sucuoglu 2006, Billington *et al*. 2009, Shing *et al*. 2009) have also indicated that wire-mesh reinforcement in various forms, even in small amounts, can significantly enhance the performance of the infilled frames as far as the damage limit state is concerned.

Carbon fiber-reinforced polymer (CFRP) strips in various arrangements have also been used to strengthen the infill panels (Erdem *et al*. 2006, Altin *et al*. 2008, Yuksel *et al*. 2010, Erol *et al*. 2012). Experimental results have indicated that CFRP strips are a viable strengthening method to increase the lateral strength and stiffness of the frames, even though, in some cases, the lateral load capacity might suddenly drop due to rupture or debonding of the CFRP, resulting in relatively low drift capacity.

Although many studies have demonstrated the possibility of increasing the strength and stiffness of an infilled RC frame, the development of brittle shear failure in the boundary columns has still not been fully addressed. Recently, a novel method of transforming the brittle behavior of the infilled RC frame to a more ductile one suitable for resisting seismic loads was proposed (Lukkunaprasit and Srechai 2012, Srechai and Lukkunaprasit 2013). The method is based on strategically modifying the load-resistance pattern and the yield mechanism of the infilled RC frame. The masonry panel is separated from the vertical columns by creating a vertical gap between the column and the infill panel so that no shear force is directly transferred to the column, eliminating the shear failure caused by the strut forces induced by the panel. Steel brackets and small vertical steel members are provided to transfer the interactive horizontal forces between the RC frame and the masonry panel and to prevent the sliding bed-joint failure of the masonry panel. The corners of the infill panel are reinforced with wire meshes and high-strength mortar to increase the compressive strength at the corners. This retrofitting scheme results in much-enhanced performance of the retrofitted structure over the un-retrofitted one, increasing the drift capacity fivefold while retaining most of the strength and stiffness.

This study focuses on further improvement of the retrofitting scheme by modifying the aspect ratio of the masonry wall and enhancing the ductility of the masonry panels with steel-wire-mesh reinforcement over the entire panel. An experiment with a large-scale specimen was carried out to verify the effectiveness of the enhanced retrofitting scheme. In addition, an analytical study was carried out to develop a computer model that provides accurate prediction of strength, stiffness, and damage pattern of the retrofitted infilled RC frame. This model can be effectively used in the global analysis of a building structure retrofitted with the proposed scheme.

2. Experimental program

In this study, a 3/4-scale model of a single-bay, single-story, non-ductile RC frame with masonry infill panel was tested under a horizontal cyclic load and a constant vertical load. The test specimen was designed based on the retrofitting concept presented by Lukkunaprasit and Srechai (2012) (Fig. 1). Strips of masonry wall adjacent to the columns were removed to create full-height openings. Steel brackets (depicted in Fig. 2) were provided to transfer the forces. Small vertical steel members (or other equivalent components) were anchored to the vertical boundaries of the masonry infill to prevent the sliding bed-joint failure of the masonry panel. The resistance capacity of the steel brackets was designed to correspond with the expected ultimate lateral capacity of the infill panel. The RC frame included typical non-ductile details used in Thailand, with minimum transverse reinforcement. Low-strength non-structural solid clay bricks were utilized to construct the 70 mm-thick infill panel (including 10 mm-thick cement plaster on each face). In this study, original brick units (130 mm×65 mm×35 mm in size) were cut to 130 mm×50 mm×35 mm corresponding to a thickness of a 3/4-scale infill panel. Four corners of the infill panel sized 500 mm×500 mm were reinforced with chicken-cage wire meshes with a reinforcement ratio of 0.29%, and high-strength mortar was applied.

Two tests were conducted using the specimen described above. In the first test, the specimen was subjected to cyclic

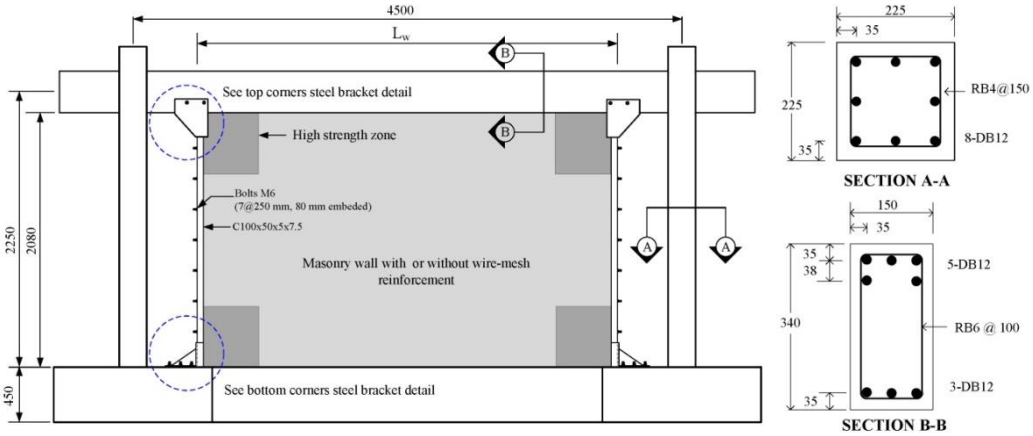

Fig. 1 Overview of the test specimen showing the retrofitting scheme (unit: mm)

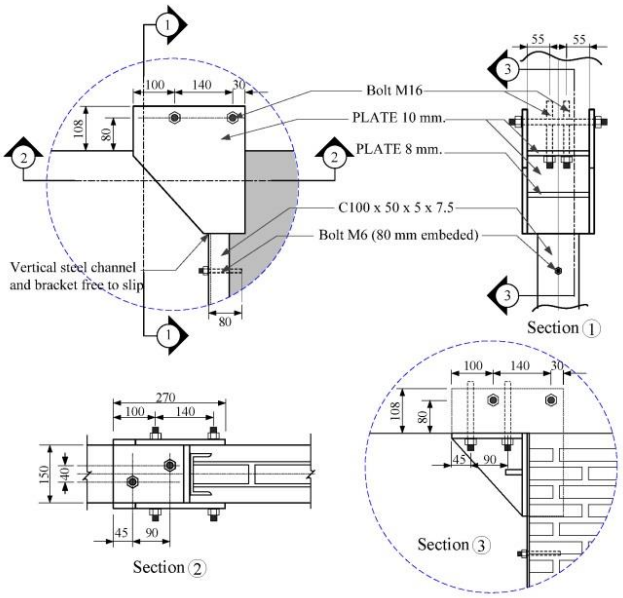

(a) top-corner bracket

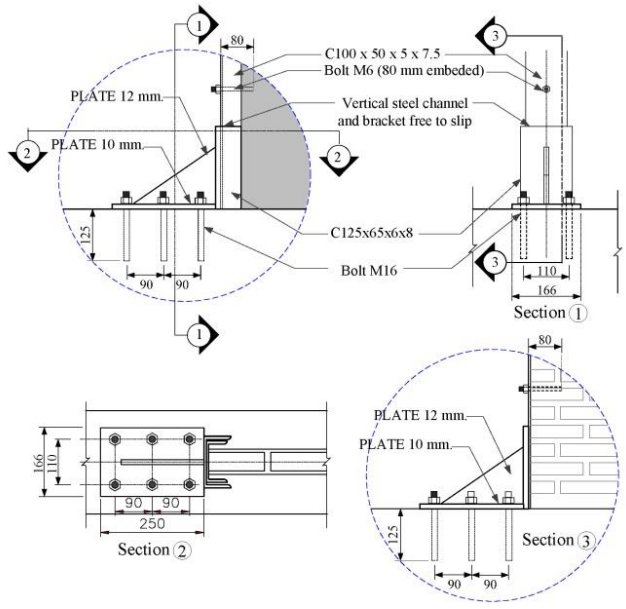

(b) bottom-corner bracket

Fig. 2 Steel bracket and connection detailing (unit: mm)

loading until failure. After the first test was completed, the specimen was repaired and subjected to a second test. The upper portion of the RC frame (including the beam) was removed and recast. The cracks elsewhere in the RC frame were repaired with high-pressure epoxy injection. The reinforcement with significant damage was replaced by a new one. The infill panel was replaced with a new one with a different aspect ratio and strength to investigate the behavior of the frame with respect to the change in infill properties. In the first test, approximately 50% of the infill panel was removed. In this paper, this original specimen with 50% removal of infill wall is designated SP50. In the second test, approximately 20% of the infill panel was removed. This repaired specimen is designated SP80. Fig. 3 shows the overview of the specimens in the first and second tests.

It is important to note that SP80 was the repaired specimen. This specimen used the reinforced infill panel covering 80% of the area, resulting in a panel aspect ratio of 0.63. In addition, steel wire mesh, 3 mm in diameter with 200×200 mm mesh, was used to reinforce the entire masonry infill panel on each face (Fig. 4). The corresponding reinforcement ratio (with respect to the horizontal area of the infill panel) was 0.11%. Small steel angles were provided to clamp the steel wire mesh to the surrounding RC frame to prevent the out-of-plane collapse of the infill panel.

Material testing was conducted prior to the commencement of the experimental program. Three types of reinforcement steel were used in each specimen: (1) 12 mm-diameter deformed bar (DB12) for longitudinal reinforcement of the RC beam and RC columns; (2) 6 mm-diameter round bar (RB6) for the transverse reinforcement of the RC beam; and (3) heat-treated 4 mm-diameter cold-drawn steel wire (RB4) for the transverse reinforcement of the RC columns. The compressive strengths of the concrete cylinder and masonry prism were also evaluated. Masonry prisms constructed from five scaled clay brick units with cement plaster on each face (130 mm×70 mm×215 mm in overall size) were tested following the ASTM-C1314-07 standard. The details of SP50 and SP80 are summarized in Table 1. It should be noted that the average modulus of elasticity of the masonry prism, obtained by compression test, was approximately 3.6 GPa.

(a) First Test (SP50)

(b) Second Test (SP80)

Fig. 3 Test specimens

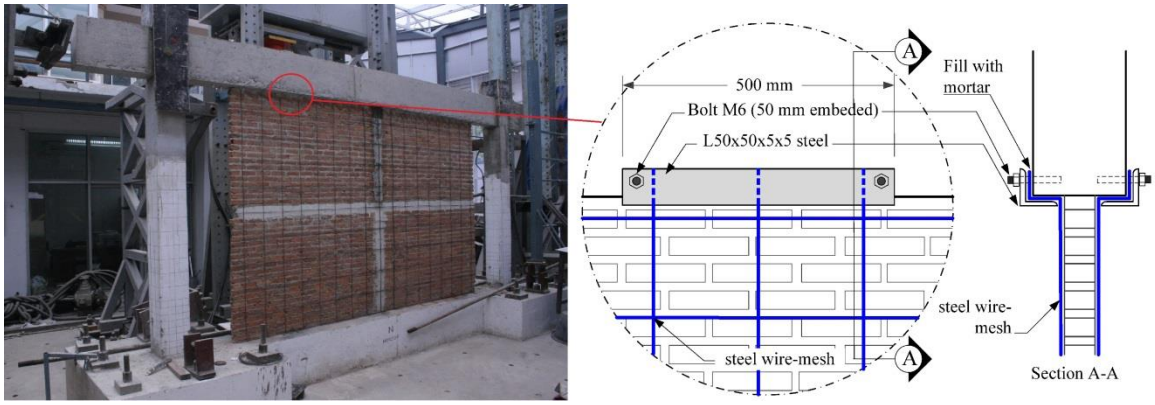

Fig. 4 URM of test specimen SP80 reinforced with steel wire mesh

Table 1 Test specimens

Specimen	Definition	Panel Aspect Ratio H_w/L_w	Masonry Strength f'_m (MPa)	Compressive strength of mortar (MPa)	Compressive strength of concrete (MPa)		Yield strength of steel reinforcement (MPa)		
					Beam	Columns	DB12	RB6	RB4
SP50	URM Panel with corner reinforcement	1.00	7.2	18.0	19.5	21.9	339.4	311.7	244.6
SP80	Panel with corner and full-panel wire-mesh reinforcement	0.63	6.9	17.4	21.6	21.6	339.4	311.7	244.6

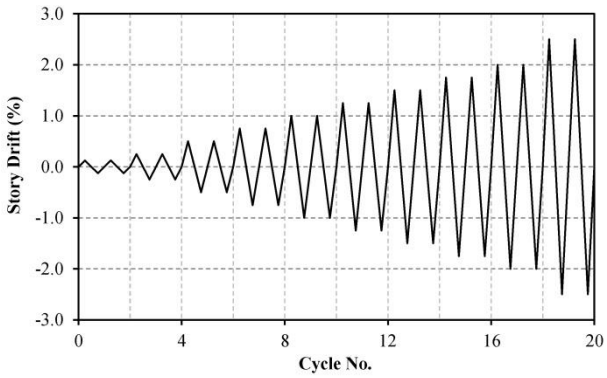

Fig. 5 Horizontal cyclic load protocol

2.1 Test setup

The tests were conducted under a horizontal cyclic load and a constant vertical load. Post-tensioned rods were used to anchor the test specimen to the strong floor. The horizontal cyclic load was applied at the centerline of the RC beam by means of a 1000 kN hydraulic actuator. The displacement-controlled loading sequence, shown in Fig. 5, was applied to the specimen. Two cycles were repeated at each drift level to ensure that stable hysteretic behavior was attained. The vertical loads of approximately 200 kN were

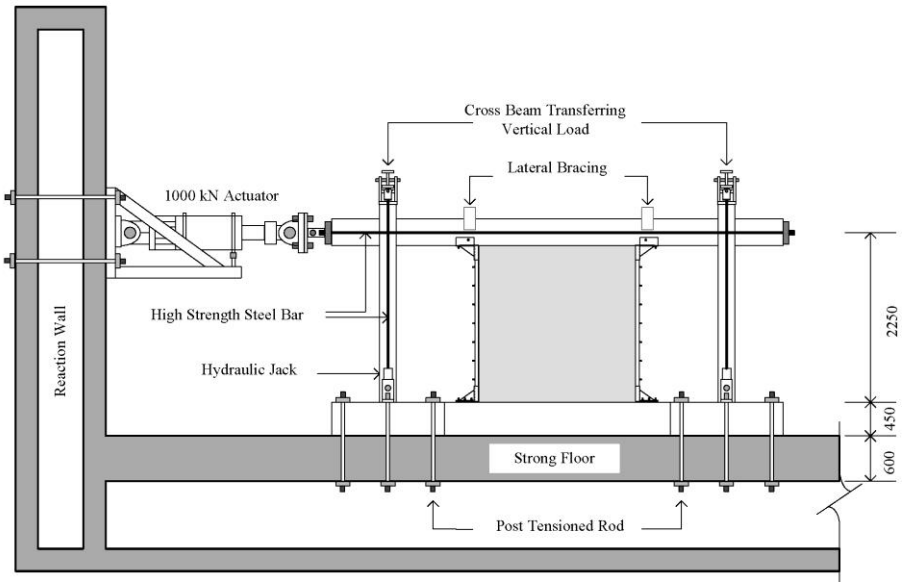

Fig. 6 Test-setup configuration (unit: mm)

applied to the tops of the columns by hydraulic jacks connected to the same hydraulic pump. During the test, those hydraulic jacks were manually controlled to maintain a constant vertical load within 5% tolerance. Strains in the longitudinal and transverse steel reinforcements of the beams and columns were monitored by strain gauges at key locations. Displacement transducers were used to measure the lateral displacement as well as the uplift of the test specimen. The test setup is illustrated in Fig. 6.

2.2 Experimental results and discussions

Fig. 7 shows the hysteretic loops of specimen SP50. This specimen, with 50% removal of the URM panel adjacent to the columns (resulting in a wall aspect ratio of 1.0), exhibited relatively ductile behavior. At 0.125% drift, a horizontal crack between the URM panel and the footing was observed. This crack opened rapidly when the test specimen was loaded to the 0.25% drift. Minor flexural cracks in the columns and beam-column joints were observed in the first cycle of the 0.5% drift. A crack width of approximately 1.0 mm was measured in the beam-column joint when the test specimen was subjected to 0.75% story drift. As depicted in Fig. 8, visible shear and flexural-shear cracks were observed in the RC beam near the load-transfer brackets at 1.0% story drift. Moreover, minor shear cracks occurred in the beam-column joints at the same state. A rocking behavior of the wall panel was clearly observed. The maximum gap between the URM panel and the footing was measured as 13 mm during the second cycle of 1.0% drift. The test specimen attained an average peak load of 173 kN at 1.50% drift.

The drift capacity achieved at a sustainable lateral load of 80% of the peak was 1.75%. Crushing of concrete in the column near the beam-column joint initiated at 1.75% drift. At a drift of 2.0%, a large diagonal crack occurred in the URM panel, resulting in a moderate drop in the lateral resistance of the test specimen. At this state, the maximum width of the diagonal crack in the infill panel was approximately 6.0 mm. The gap at the base of the wall was measured as 26 mm. The damage condition of specimen SP50 at 2.0% story drift is shown in Fig. 9. At a drift of 2.5%, severe crushing and splitting of concrete in the column near the beam-column joint occurred. After that, the longitudinal steel bars in the column buckled. The gap at the base of the wall due to rocking widened to as large as 30 mm at this state.

Fig. 10 shows the hysteretic loops of specimen SP80. At 0.125% drift, small diagonal cracks started to develop in the panel. The crack width of approximately 0.5 mm was

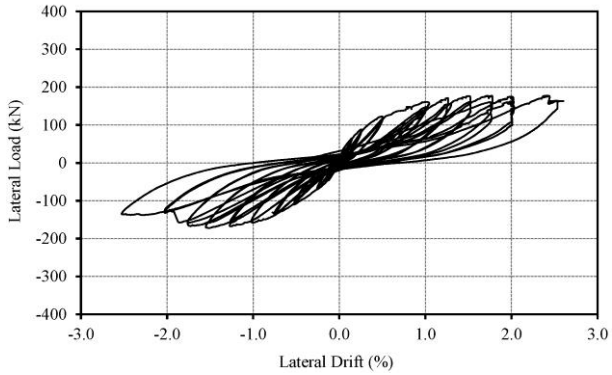

Fig. 7 Hysteretic loops of the retrofitted specimen SP50

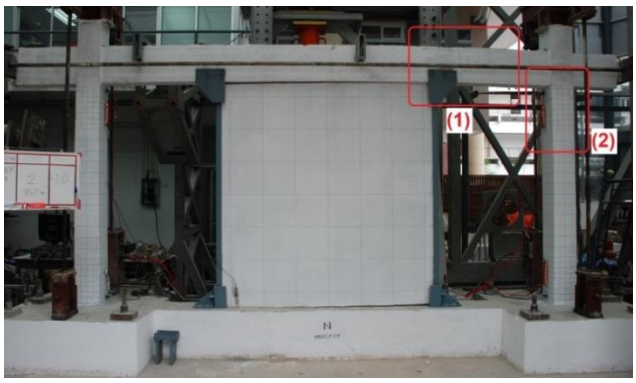

(a) Overview

(b) Region 1

(c) Region 2

Fig. 8 Damage condition of specimen SP50 at 1.00% drift

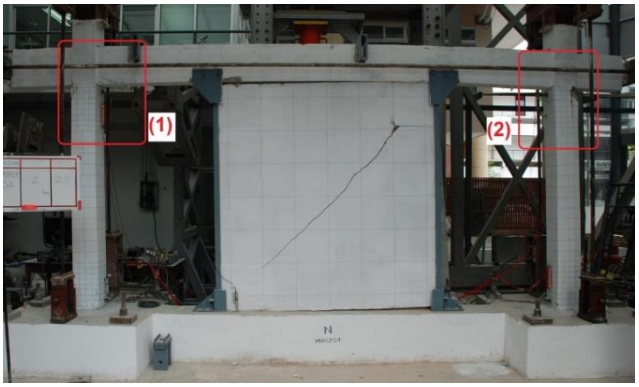

(a) Overview

(b) Region 1

(c) Region 2

Fig. 9 Damage condition of specimen SP50 at 2.00% drift

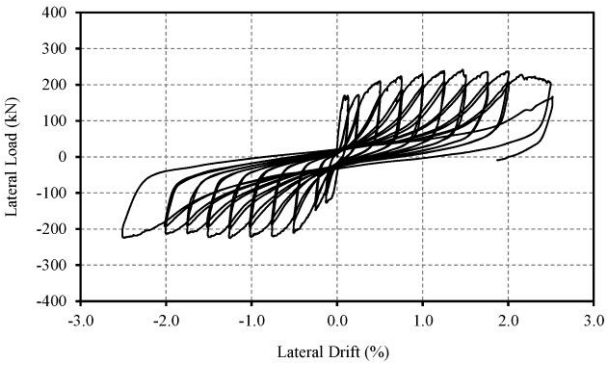

Fig. 10 Hysteretic loops of the retrofitted specimen SP80

(a) Overview

(b) Left beam-to-column connection

(c) Left column

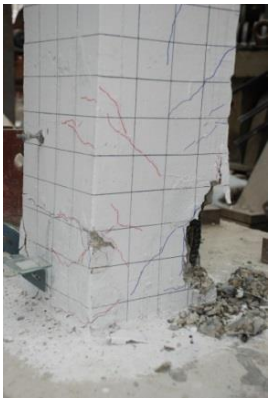

(d) Right column

(e) Right beam-to-column connection

Fig. 11 Damage condition of specimen SP80 at 2.5% drift

measured. When the test specimen was loaded to 0.25% drift, hairline flexural cracks occurred in the RC columns. A slight corner crushing of the infill panel developed at 0.50% drift. Moreover, at this state, the steel wires attached to the surrounding RC frame were pulled out due to sliding of the infill panel. A small diagonal crack was observed at the corner of the infill panel during the first cycle to 0.75% drift. Visible flexural-shear cracks developed in the RC columns. During the second cycle of 0.75% drift, the largest crack in the RC columns widened to approximately 0.5 mm. The test specimen approximately maintained an average peak load of 230 kN at 1.25% drift up to 2.00% drift. The specimen could sustain a drift capacity of 2.0% at a lateral load of over 80% of the peak load (see Fig. 10). At 1.75% drift, the largest crack in the RC columns was approximately 1.0 mm wide. Additionally, the gap between the wall and footing due to rocking was 4 mm. It was observed that with a slight steel wire-mesh reinforcement in the infill panel, the damage to the infill panel was reduced considerably. At 2.0% drift, crushing of concrete in the RC column near the footing and spalling of cement plaster at the corner of the infill panel were observed. At this state, the test specimen was able to sustain a lateral load of approximately 90% of the peak capacity. Finally, the flexural-shear failure occurred abruptly at the lower part of the RC column during the second cycle of 2.5% drift, as depicted in Fig. 11.

The envelope curves of lateral load versus drift ratio from the two tests are shown in Fig. 12. The figure also shows the envelope curve of the specimen with full infill panel (100% infilled) tested by Srechai and Lukkunaprasit (2013), which represents the condition of the frame before retrofitting without removal of the infill-panel edges. The test results of the un-retrofitted infilled frame (fully infilled frame) are described in detail in Srechai and Lukkunaprasit (2013). Overall, specimens SP50 and SP80 exhibited remarkable improvements in performance over the specimen tested by Srechai and Lukkunaprasit (2013). The average peak lateral load of SP80 was 0.79 times that of the fully infilled specimen. However, the drift capacity of SP80 at a sustainable lateral load of 80% of the peak load was 8 times larger. Furthermore, specimen SP80 exhibited less strength degradation. Similarly, the average peak strength of specimen SP50 was only 0.59 times that of the fully infilled specimen, while the drift capacity was 7 times larger. This clearly illustrates the effectiveness of the retrofitting method in increasing the ductility of the frame. It is also interesting to note that the reduction in the URM panel area results in an approximately proportional decrease in the peak lateral load. This can be used as a preliminary design guide to select the infill-wall area reduction given the required overall strength of the frame.

Fig. 13 compares the secant stiffness versus drift ratios of the tested specimens. At 0.125% drift, the secant stiffness of specimen SP80 was approximately 82% of that of the fully infilled specimen tested by Srechai and Lukkunaprasit (2013). However, it reduced to 64% at 0.25% drift. With the removal of 50% of the URM infill panel (specimen SP50), the secant stiffness at 0.125% drift was only 30% of that of the un-retrofitted specimen. This significant reduction in the stiffness of specimen SP50 was caused by the rocking

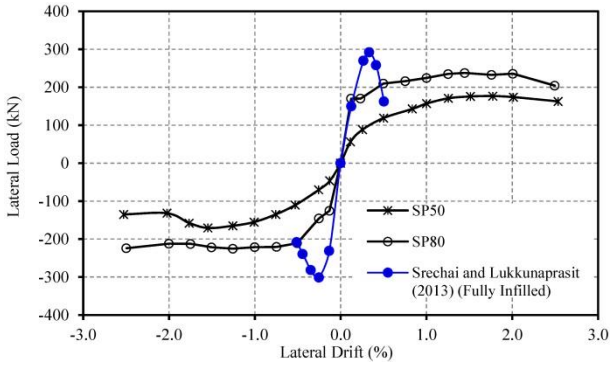

Fig. 12 Envelopes of the hysteretic curves

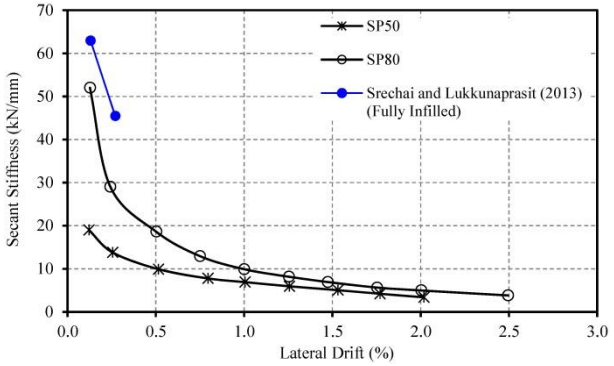

Fig. 13 Secant-stiffness variation with lateral drift

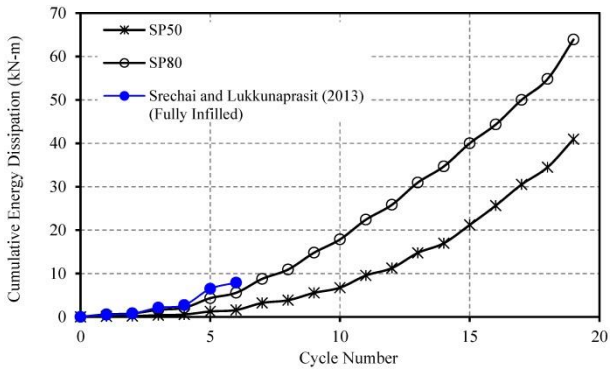

Fig. 14 Cumulative energy dissipation with loading cycles

motion of the URM panel. As the area reduction becomes larger, the aspect ratio of the remaining panel increases. This increases the rocking motion of the panel, resulting in larger lateral drift and smaller stiffness.

One of the key characteristics of seismic-resistant structures is the ability to dissipate energy. The energy-dissipation capacities, as calculated from the areas under the hysteretic loops, are presented in Fig. 14. The retrofitted specimens provided higher total energy-dissipation capacities than the un-retrofitted specimen, even though the strength and stiffness were lower. The energy-dissipation capacity of specimen SP50 was lower than that of SP80 because its lateral strength was significantly lower (0.75 times) than that of specimen SP80.

The performance of the specimens can be characterized based on force-deformation curves, as recommended by ASCE41-06 (ASCE, 2007). For reinforced concrete frames

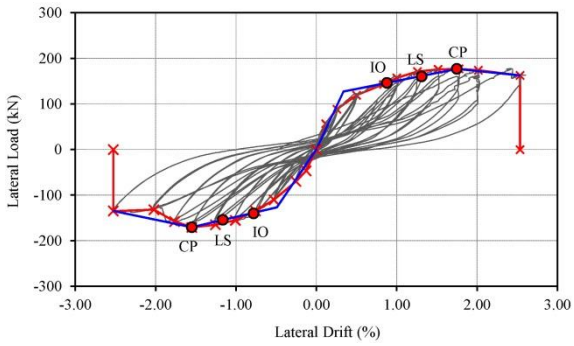

(a) SP50

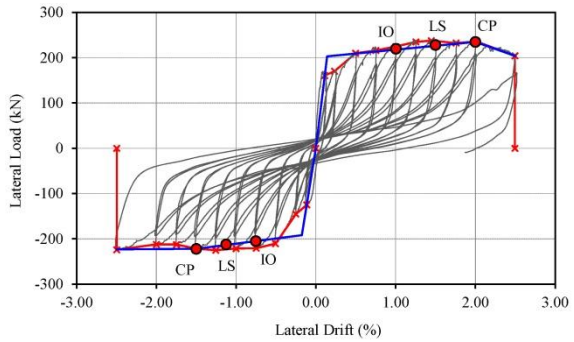

(b) SP80

Fig. 15 Performance levels of specimens

with masonry infills, Collapse Prevention (CP) Performance Level is defined as the state at which strength degradation begins, Life Safety (LS) Performance Level is taken as 3/4 of the deformation at CP, and Immediate Occupancy (IO) Performance Level is taken as 2/3 of the deformation at LS. The performance levels are shown in Fig. 15.

At the LS level, specimen SP50 could sustain an average lateral drift of approximately 1.24%, close to the drift at peak capacity, with stable hysteretic behavior. The drift capacity at CP level was 1.65%. At LS level, flexural cracks, with the largest one being approximately 1 mm wide, and visible shear cracks developed in the surrounding RC frame. The URM infill suffered no diagonal cracks at this level. However, significant rocking occurred, resulting in some crushing at one corner. For specimen SP80, the performance level was determined to be LS at an average lateral drift of approximately 1.31% and CP at the drift capacity of 1.75%. At the LS level, the test specimen had already reached its peak lateral capacity with only a slight strength degradation. Furthermore, only minor flexural and flexural-shear cracks (approximately 0.5 mm in width) developed in the surrounding RC frame with no sign of distress. Only minor diagonal cracks formed in the URM infill and minor corner crushing developed.

In comparison, both retrofitted specimens clearly performed significantly better than the URM infill-wall deformation limit of 0.5% at the LS level as specified in ASCE41-06. Similarly, Eurocode 8 (Eurocode, 2004) specifies a story drift limit of 0.5% corresponding to the no-collapse state for structures with brittle non-structural elements attached to the frame.

3. Analytical study

A macro-scale computer model capable of representing the strength, stiffness, and damage pattern of the retrofitted infilled RC frame was developed. This model could be used effectively in the global analysis of a building structure retrofitted with the proposed scheme. In the literature, a number of analytical approaches for RC frames with masonry infill panels have been proposed. However, only an effective and practical approach based on the equivalent diagonal strut concept is adopted in this study. The details of the analytical model and some analytical results are described in the following sections and compared to those from the tests.

3.1 Model description and calibration

A non-linear analytical model of the RC frame with masonry-infilled wall was constructed as depicted in Fig. 16. The columns and beam were modeled using lump-plasticity frame elements with an effective stiffness. The axial load-moment interaction flexural plastic hinge was introduced at each end of the columns. To represent the shear capacity of the columns, shear plastic hinges were introduced at one end of the column members. In the case of the beam, only the flexural plastic hinges were used. The beam-column joints were treated as rigid. The center and exterior struts were assigned 60% and 20% of the total width and capacity, respectively. The exterior struts were connected to the steel bracket at one end and to the base at the other end. The end points located at the points indicated by the diagonal dashed lines shown in the figure. Each dashed line initiated from a point at a distance of $Z/2$ from the end of the column or the bottom face of the beam and inclined with the same slope as the central-strut. The distance Z is the contact length between the RC columns and URM panel (for fully infilled frame) according to Smith and Carter (1969).

For flexural nonlinearity, an effective plastic-hinge moment-rotation relation proposed by Haselton and Deierlein (2007) was used. Overall effects of concrete crushing, steel-reinforcement buckling, and bond failure of rebar were included in this model. The flexural plastic-hinge load-deformation curve was tri-linear (Fig. 17(a)). The response was linearly elastic up to the yield moment (M_y). In this range, the lateral stiffness of the element was defined as the effective stiffness. Afterwards, the load gradually increased until reaching the maximum moment (M_c) at the corresponding chord rotation (θ_{cap}). At θ_{cap}, the strength degraded with softening stiffness (K_c) until the moment capacity became zero.

For the shear plastic hinge, a model proposed by Patwardhan (2005) was modified and used in this study. The load-displacement relation of the shear plastic hinge by Patwardhan (2005) is depicted in Fig. 17(b). The shear-plastic-hinge load-deformation curve is quad-linear. The response is linearly elastic up to the cracking strength (V_{cr}) at the cracking displacement ($\Delta_{v,cr}$). Beyond this level, the shear strength increases until reaching the maximum capacity (V_n) at the corresponding displacement ($\Delta_{v,n}$). The shear strength remains constant until the onset of shear-strength degradation. After this level, the shear strength rapidly reduces to zero when axial load failure occurs. However, to simplify the analysis, a tri-linear load-displacement curve excluding the cracking point was used instead of the quad-linear model.

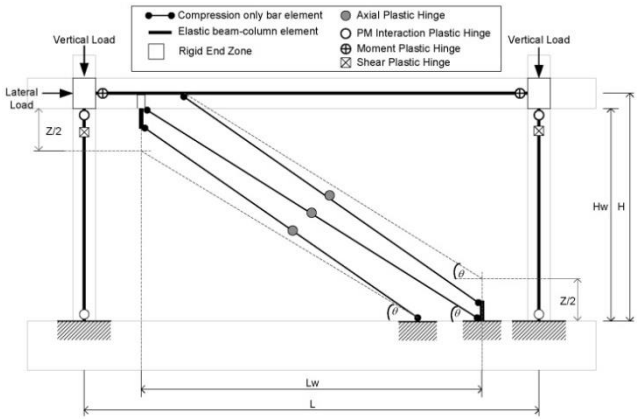

Fig. 16 Analytical model of retrofitted specimen

For the masonry infill panel, a simplified lateral load-deformation relation of the panel, specified by ASCE41-06 (ASCE, 2007), was modified and utilized in the analytical model. Fig. 17(c) shows the skeleton of the masonry-infill-panel load-deformation relation. The load-deformation curve consists of four linear segments. The response is elastic up to the yield strength. After this point, the load gradually increases until it reaches the maximum strength (V_{max}) at the corresponding lateral displacement (Δ_{max}). At Δ_{max}, the strength degrades with softening stiffness (K_{sof}) until reaching the residual strength (V_{res}). After this point, the strength is assumed to be constant. The necessary parameters to construct the curve include the following:

• Initial stiffness (K_{ini})

The initial stiffness of the masonry infill panel represents the elastic stiffness of the panel and can be determined by the method introduced by Fiorato *et al.* (1970) based on the conventional principle of mechanics. The initial lateral stiffness of the masonry infill panel can be expressed as

$$K_{ini} = \frac{1}{\frac{1}{K_{fl}} + \frac{1}{K_{sh}}} \tag{1}$$

where K_{fl} and K_{sh} are the flexural and shear stiffnesses of a cantilever masonry panel, respectively, given by

$$K_{fl} = \frac{3E_m I_w}{h_w^3} \tag{2}$$

$$K_{sh} = \frac{A_w G_w}{h_w} \tag{3}$$

where E_m, I_w, h_w, A_w, and G_w are the modulus of elasticity, moment of inertia, height, cross-sectional area, and shear modulus of the masonry panel. The shear modulus of the masonry infill panel can be assumed as $0.4E_m$ (Stavridis and Shing 2012). The computed stiffness value can be used in assigning the area of the equivalent strut.

• Yield strength (V_y)

According to an extensive literature review by Uva *et al.* (2012), the yield capacity of the masonry infill panel ranges from 0.6 to 0.8 times the maximum capacity. In this research, the yield strength of the masonry infill panel is assumed to be 0.8 times the maximum capacity.

•Maximum strength (V_{max})

According to Asteris *et al.* (2011), sliding along the bed joint and corner crushing of the masonry infill panels are the predominant failure modes. Therefore, the lateral capacity of the masonry infill panel can be approximately taken as the smaller of the capacities associated with these two failure modes. The approach developed by Mostafaei and Kabeyasawa (2004) was used to estimate the lateral capacity of sliding along the bed-joint failure mode (V_{slide}). For the corner-crushing failure mode (V_{cc}), the total effective width of the diagonal struts (w) was calculated following the method proposed by Mainstone (1971).

• Lateral drift at maximum strength (Δ_{max})

In this research, the lateral deformation at maximum capacity of the masonry infill panel is estimated following the recommendation of the ASCE41-06 standard (ASCE, 2007). Since the test results revealed much improved displacement ductility, a trial and error approach was used to estimate the drift at maximum capacity of the masonry infill panel. The drift Δ_{max} of approximately 2 times the ASCE41-06 recommended value yields reasonable agreement with the experimental results.

• Residual strength (V_{res}) and the associated lateral drift (Δ_{res})

As mentioned earlier, the strength and deformation of the masonry infill panel depend on its failure mode. Therefore, the actual residual strength and deformation at residual strength cannot be estimated using a simple methodology. A number of researchers assume the residual capacity of the masonry infill panel as a fraction of the maximum capacity, ranging from 0 to 0.35 times the maximum capacity (Uva *et al.* 2012). The associated lateral drift can be calculated by assuming the softening stiffness (K_{sof}) of the masonry infill panel as a fraction of the initial stiffness. Uva *et al.* (2012), based on the suggestion of Panagiotakos and Fardis (1996), proposed a range of softening stiffness from 0.005 to 0.1 times the initial stiffness. In this research, the residual capacity of the masonry infill panel was assumed to be 0.2 times the maximum capacity. For the softening stiffness, it was found that the aspect ratio of the infill panel had a strong influence. The value of the softening stiffness should, therefore, be assigned according the aspect ratio of the infill panel. This issue is explored further in the next section.

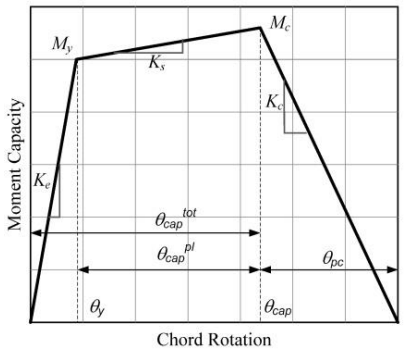

(a) Flexural plastic hinge

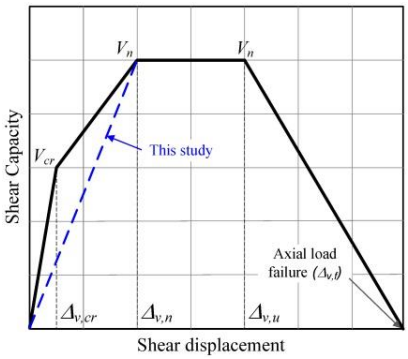

(b) Shear plastic hinge

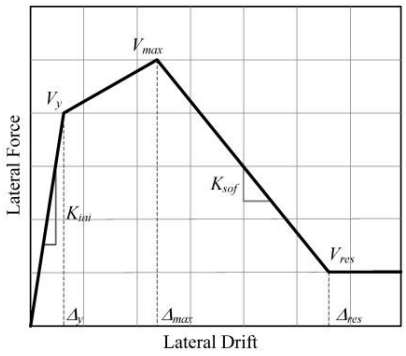

(c) Masonry infill panel

Fig. 17 Load-deformation relations of plastic hinges and masonry infill panel

3.2 Results and discussion

Based on the approach described above, analytical models of SP50 and SP80 were constructed. Table 2 summarizes the values of different parameters assigned to the models. Softening stiffness (K_{sof}) values from 1% to 5% of the initial stiffness were assigned to investigate the sensitivity of the analysis results. It should be noted that all values shown in the table except w were defined for the horizontal direction. Therefore, all parameters must be

Table 2 Masonry-infill-panel model properties of retrofitted specimens

Specimen	Properties									
	w (mm)	V_{slide} (kN)	V_{cc} (kN)	K_{ini} (kN/mm)	V_{max} (kN)	V_y (kN)	V_{res} (kN)	Δ_y (mm)	Δ_{max} (mm)	Δ_{res} (mm)
SP50	309	334	**106**	39	106	85	21	2.18	33.28	106.77
SP80	426	264	**183**	108	183	146	37	1.35	13.93	149.76

transformed into those for the direction of the diagonal strut before using them in the strut model.

Fig. 18 shows the comparison of the lateral force versus story drift relations of specimen SP50 between the test and analysis results. Damage patterns corresponding to important states are also shown in the figure. It can be seen that the analytical initial stiffness matched well with the experimental result when the story drift was smaller than 0.125%. After this state, the analytical lateral stiffness was measurably larger than the experimentally obtained value. However, after an interior diagonal strut yielded (point 1), the lateral stiffness of the specimen decreased considerably. Moreover, when the yielding initiated in an exterior diagonal strut (point 2), the analytical lateral stiffness of the specimen was consistent with the experimental result. The analytical results indicated that the specimen reached its peak lateral load at 0.9% drift. This story drift was considerably smaller than the experimentally observed value. However, the analytical model could capture the average peak lateral load of the specimen. For an infill panel with high aspect ratio such as this one, the softening of the infill struts had a minor influence on the overall load resistance of the frame for the range of story drifts relevant for practical purposes. The softening stiffnesses between 1-5% all yielded similar results, except for drift values larger than 2.5%, i.e., beyond the drift limit obtained from the test. The softening of lateral stiffness obtained by the analytical procedure reasonably matched the experimental envelope curves. According to the experimental results, only flexural yielding was observed in the RC columns, which is consistent with the analytical result.

The lateral force versus story drift relations of specimen SP80 from the analysis and the test are illustrated in Fig. 19. It can be seen that the analytical initial stiffness matched well with the experimental result, especially when compared with the experimental positive-envelope curve. However, the analytical initial stiffness was considerably larger when compared with the experimental negative-envelope curve. The experimental results revealed that the lateral strength of the tested specimen slightly dropped due to diagonal cracking of the infill panel. At a similar story drift, yielding of the bottom exterior and interior diagonal struts (point 2) was observed in the analytical investigation. Consequently, the lateral stiffness of specimen SP80 considerably decreased without lateral-strength deterioration. The proposed analytical model accurately captured the lateral-strength deterioration caused by a diagonal crack in the infill panel. The analytical result shows that the specimen reached its peak lateral load at approximately 1.15% drift. This drift was slightly smaller than the experimental result. Moreover, the peak lateral strength obtained by the analytical procedure was slightly higher than the experimentally obtained value. This is due to the large variation inherent in the strength calculation of the infill panel. The lateral-strength deterioration of the analytical curve was observed at 1.5% drift, which agrees reasonably well with the experimental curves. For the infill panel with low aspect ratio, the softening stiffness had a

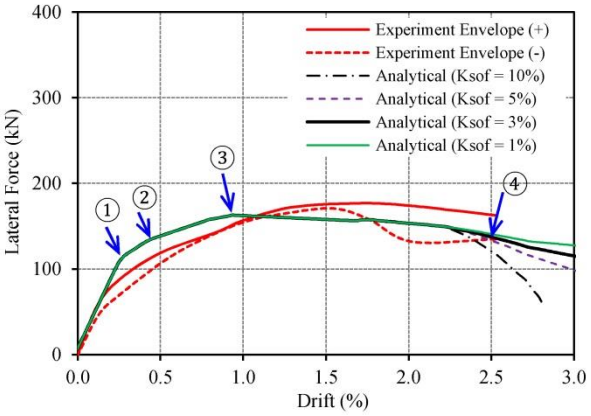

(a) Lateral force versus story drift

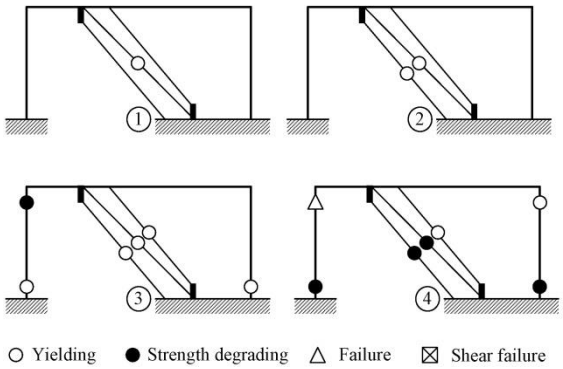

(b) Damage pattern

Fig. 18 Analytical results of specimen SP50

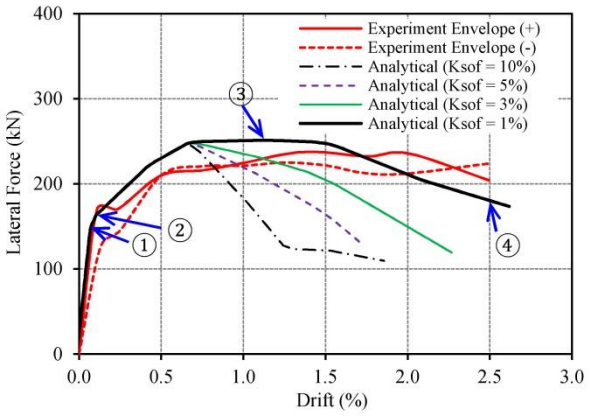

(a) Lateral force versus story drift

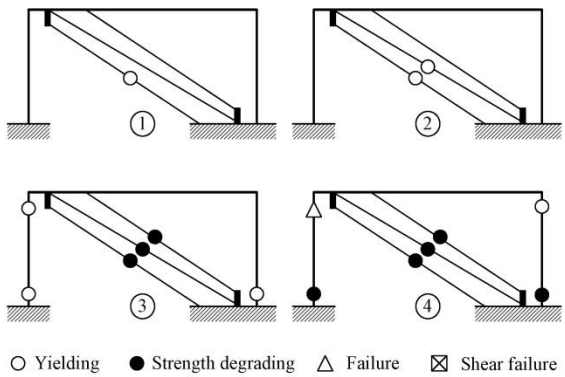

(b) Damage pattern

Fig. 19 Analytical results of specimen SP80

very large influence on the overall load resistance of the frame. Softening between 1-5% produced significantly different results. In addition, the steel wire-mesh reinforcement employed in the infill panel significantly improved the ductility, leading to a much more gradual drop in the peak load. A low value of softening stiffness of 1% appeared to match the experimental envelope curves for this case.

As reported by Chiou and Hwang (2015), the aspect ratio of an infill panel can significantly affect the response of the frame. In this retrofitting scheme, for the panel with low aspect ratio (SP80), the inclination angle of the diagonal strut from the horizontal direction (θ) was relatively small. As a result, the horizontal component of strut force was significantly large. Any softening in the infill stiffness would considerably affect the lateral load carrying mechanism and overall lateral load resistance of the frame. On the other hand, the panel with high aspect ratio (SP50) involved greater rocking response of the infill panel and less contribution from the horizontal component of the strut force. The softening in the infill stiffness thus played a less important role in the overall lateral load resistance of the frame.

4. Conclusions

Experimental and analytical evaluations of an effective approach for the retrofitting of masonry-infilled non-ductile RC frame were carried out in this study. The retrofitting scheme was based on the concept proposed by Lukkunaprasit and Srechai (2012) with additional improvements. Quasi-static tests were performed to evaluate the effectiveness of the proposed method. In addition, a computer model using a diagonal-struts concept for predicting the global behavior of the structures was developed and calibrated experimentally. The main findings are summarized as follows:

- The retrofitted specimens exhibited remarkable improvements in performance over the un-retrofitted specimen (fully infilled), especially in terms of the ductility. The retrofitted specimens achieved drift capacities approximately 7 times larger than that of the un-retrofitted one. In addition, a small amount of steel wire-mesh reinforcement in the infill panel could reduce the damage and further enhance the ductility of the masonry infill panel.
- The peak lateral load resistance of the frame decreased approximately in proportion to the width reduction of the infill panel. In addition, increasing the aspect ratio of the infill panel resulted in rocking motion of the panel, which significantly affected the stiffness of the frame. Therefore, in a real application, the retrofitting design must be carefully checked with a suitable computer model with regards to the balance between strength, stiffness, and ductility.
- The analytical model presented in this study could predict the global responses of the tested specimens reasonably well, especially in terms of strength, stiffness and damage pattern. For prediction of the peak capacities of the test specimens, a slight error within 3% to 8%, compared with the average peak capacities obtained from the experiments, could be achieved. For an infill panel with a low aspect ratio, the softening stiffness of the masonry panel is an important parameter that had a significant influence on the overall load resistance of the frame. For the specimen investigated in this study, a softening stiffness of 1% of the initial stiffness could account for the gradual drop in the descending branch of the load-deformation curve.
- In this study, a drift at maximum capacity of the masonry infill panel of approximately 2 times the value recommended in ASCE41-06 yielded reasonable agreement with the experimental results.

Acknowledgments

The authors are grateful for funding from the Commission on Higher Education of Thailand-AUN/SEED-Net and Faculty of Engineering, Burapha University, Thailand (No. CA2/2553). The general support from Chulalongkorn University to the Center of Excellence in Earthquake Engineering and Vibration is acknowledged. The assistance of Building 33 Company Limited in casting the test specimens is greatly appreciated.

References

ACI 318 (2008), Building code requirements for structural concrete and commentary, American Concrete Institute, Farmington Hills, MI

Acun, B. and Sucuoglu, H. (2006), "Strengthening of masonry infill walls in reinforced concrete frames with wire mesh reinforcement", *8th US National Conference on Earthquake Engineering*, San Francisco, CA, April.

Al-Chaar, G., Issa, M. and Sweeney, S. (2002), "Behavior of masonry-infilled nonductile reinforced concrete frames", *J. Struct. Eng.*, **128**(8), 1055-1063.

Altin, S., Anil, Ö., Kara, M.E. and Kaya, M. (2008), "An experimental study on strengthening of masonry infilled rc frames using diagonal cfrp strips", *Compos. Part B: Eng.*, **39**(4), 680-693.

ASCE41-06 (2007), Seismic rehabilitation of existing buildings, American Society of Civil Engineers, Reston, VA.

Asteris, P.G., Antoniou, S.T., Sophianopoulos, D.S. and Chrysostomou, C.Z. (2011), "Mathematical macromodeling of infilled frames: State of the art", *J. Struct. Eng.*, **137**(12), 1508-1517.

ASTM (2007), Standard test method for compressive strength of masonry prisms (ASTM C1314), ASTM International, West Conshohocken, PA.

Bertero, V. and Brokken, S. (1983), "Infills in seismic resistant building", *J. Struct. Eng.*, **109**(6), 1337-1361.

Billington, S., Kyriakides, M., Blackard, B., Willam, K., Stavridis, A. and Shing, P. (2009), "Evaluation of a sprayable, ductile cement-based composite for the seismic retrofit of unreinforced masonry infills", *Improving the seismic performance of existing buildings and other structures*, San Francisco, CA, December.

Calvi, G.M. and Bolognini, D. (2001), "Seismic response of reinforced concrete frames infilled with weakly reinforced masonry panels", *J. Earthq. Eng.*, **5**(2), 153-185.

Chiou, T.C. and S.J. Hwang (2015), "Tests on cyclic behavior of

reinforced concrete frames with brick infill", *Earthq. Eng. Struct. D.*, **44**(12), 1939-1958.
Corte, G.D., Fiorino, L. and Mazzolani, F. (2008), "Lateral-loading tests on a real rc building including masonry infill panels with and without frp strengthening", *J. Mater. Civ. Eng.*, **20**(6), 419-431.
Elwood, K.J. and Moehle, J.P. (2005), "Axial capacity model for shear-damaged columns", *ACI Struct. J.*, **102**(4), 578-587.
Eurocode (2004), Design of structures for earthquake resistance. Part 1: General rules, Seismic actions and Rules for buildings, European Committee for Standardization; Brussels, Belgium.
Erdem, I., Akyuz, U., Ersoy, U. and Ozcebe, G. (2006), "An experimental study on two different strengthening techniques for rc frames", *Eng. Struct.*, **28**(13), 1843-1851.
Erol, G., Karadogan, H.F. and Cili, F. (2012), "Seismic strengthening of infilled reinforced concrete frames by cfrp", *15th World Conference on Earthquake Engineering*, Lisbon, Portugal, September.
Fardis, M.N. and Panagiotakos, T.B. (1997), "Seismic design and response of bare and masonry-infilled reinforced concrete buildings. Part II: Infilled structures", *J. Earthq. Eng.*, **1**(3), 475-503.
FEMA (1998), Evaluation of earthquake-damaged concrete and masonry wall building-basic procedures manual, Federal Emergency Management Agency,Washington, D.C.
Fiorato, A.E., Sozen, M.A. and Gamble, W.L. (1970), "An investigation on the interaction of reinforced concrete frames with masonry filler walls", Report UILU-ENG 70-100, University of Illinois - Urbana Champaign, IL.
Gómez-Martínez, F., Pérez-García, A., De Luca, F., Verderame, G. M. and Manfredi, G. (2012), "Preliminary study of the structural role played by masonry infills on rc building performances after the 2011 lorca, spain, earthquake", *15th World Conference on Earthquake Engineering*, Lisbon, Portugal, September.
Haselton, C.B. and Deierlein, G.G. (2007), "Assessing seismic collapse safety of modern reinforced concrete momentframe buildings", Report No. 152, John A. Blume Earthquake Engineering Center, Stanford University, CA.
Hassan, A.F. and Sozen, M.A. (1997), "Seismic vulnerability assessment of low-rise buildings in regions with infrequent earthquakes", *ACI Struct. J.*, **94**(1), 31-39.
Kyriakides, M.A. and Billington, S.L. (2008), "Seismic retrofit of masonry-infilled non-ductile reinforced concrete frames using sprayable ecc", *14th World Conference on Earthquake Engineering*, Beijing, China, October.
Lee, H.S. and Woo, S. (2002), "Effect of masonry infills on seismic performance of a 3-storey r/c frame with non-seismic detailing", *Earthq. Eng. Struct. D.*, **31**(2), 353-378.
Lukkunaprasit, P. and Srechai, J. (2012), "A low cost retrofit scheme for masonry-infilled non-ductile reinforced concrete frames", *15th World Conference on Earthquake Engineering*, Lisbon, Portugal, September.
Lukkunaprasit, P., Ruangrassamee, A., Boonyatee, T., Chintanapakdee, C., Jankaew, K., Thanasisathit, N. and Chandrangsu, T. (2016), "Performance of structures in the Mw 6.1 Mae Lao earthquake in Thailand on May 5, 2014 and implications for future construction", *J. Earthq. Eng.*, **20**(2), 219-242.
Mainstone, R.J. (1971), "On the stiffnesses and strengths of infilled frames", *Proceedings of the Institution of Civil Engineers*, Supplement (iv), 57-90.
Mehrabi, A., Benson Shing, P., Schuller, M. and Noland, J. (1996), "Experimental evaluation of masonry-infilled rc frames", *J. Struct. Eng.*, **122**(3), 228-237.
Mostafaei, H. and Kabeyasawa, T. (2004), "Effect of infill masonry walls on the seismic response of reinforced concrete buildings subjected to the 2003 bam earthquake strong motion: A case study of bam telephone center", *Bull. Earthq. Res. Inst.*, **79**(3), 133-156.
Panagiotakos, T.B. and Fardis, M.N. (1996), "Seismic response of infilled rc frames structures", *11th World Conference on Earthquake Engineering*, Acapulco, Mexico, June.
Patwardhan, C. (2005), "Shear strength and deformation modeling of reinforced concrete columns", Master Thesis, The Ohio State University, OH.
Paulay, T. and Priestly, M.J.N. (1992), *Seismic Design of Reinforced Concrete and Masonry Buildings*, John Wiley & Sons, NY.
Pinto, A.V. and Taucer, F. (2006), "Assessment and retrofit of full-scale models of existing rc frames", *Advances in Earthquake Engineering for Urban Risk Reduction*, Springer, Dordrecht.
Pujol, S. and Fick, D. (2010), "The test of a full-scale three-story rc structure with masonry infill walls", *Eng. Struct.*, **32**(10), 3112-3121.
Sezen, H., Whittaker, A.S., Elwood, K.J. and Mosalam, K.M. (2003), "Performance of reinforced concrete buildings during the august 17, 1999 Kocaeli, turkey earthquake, and seismic design and construction practise in turkey", *Eng. Struct.*, **25**(1), 103-114.
Shing, P., Stavridis, A., Koutromanos, I., Willam, K., Blackard, B., Kyriakides, M., Billington, S. and Arnold, S. (2009), "Seismic performance of non-ductile rc frames with brick infill", *Improving the seismic performance of existing buildings and other structures*, San Francisco, CA, December.
Shing, P.B. and Mehrabi, A.B. (2002), "Behaviour and analysis of masonry-infilled frames", *Progr. Struct. Eng. Mater*, **4**(3), 320-331.
Srechai, J. and Lukkunaprasit, P. (2013), "An innovative scheme for retrofitting masonry-infilled non-ductile reinforced concrete frames", *The IES J. Part A: Civ. Struct. Eng.*, **6**(4), 277-289.
Smith, B.S., and Carter, C. (1969), "A method of analysis for infilled frames", *Proc. Inst. Civ. Engineers*, **44**(1), 31-48.
Stavridis, A. and Shing, P.B. (2012), "Simplified modeling of masonry-infilled rc frames subjected to seismic loads", *15th World Conference on Earthquake Engineering*, Lisbon, Portugal, September.
Uva, G., Raffaele, D., Porco, F. and Fiore, A. (2012), "On the role of equivalent strut models in the seismic assessment of infilled rc buildings", *Eng. Struct.*, **42**, 83-94.
Yuksel, E., Ozkaynak, H., Buyukozturk, O., Yalcin, C., Dindar, A. A., Surmeli, M. and Tastan, D. (2010), "Performance of alternative cfrp retrofitting schemes used in infilled rc frames", *Constr. Build. Mater.*, **24**(4), 596-609.

KT

Appendix

The equations employed to calculate the key parameters in the analytical model can be summarized as follows:

• Flexural plastic hinge properties

The yielding moment (M_y) can be determined by several approaches. Once it is determined, the maximum moment (M_c) can be computed from the ratio between M_c and M_y according to Haselton and Deierlein (2007)

$$\frac{M_c}{M_y} = (1.25)(0.89)^{v}(0.91)^{1.0\,1c_{units}f_c'} \tag{A1}$$

where v is the axial load ratio ($P/A_g\ f_c'$), P is the axial load, A_g is a gross-sectional area of column, c_{units} is a unit conversion variable equal to 1.0 when the unit is MPa, and f'_c is concrete compressive strength (MPa).

The post-yielding stiffness (K_s) and the softening stiffness (K_c) can be expressed as

$$K_s = \frac{M_c - M_y}{\theta_{cap}^{\ pl}} \tag{A2}$$

and

$$K_c = \frac{M_c}{\theta_{pc}} \tag{A3}$$

where $\theta_{cap}^{\ pl}$ and θ_{pc} are determined by empirical equations given in terms of longitudinal and transverse reinforcement ratios, rebar yield strength, and the diameter and arrangement of rebars (Haselton and Deierlein 2007).

• Shear plastic hinge properties

The maximum shear strength (V_n) suggested by ACI 318 (2008) was used in this study. According to Patwardhan (2005), the corresponding shear displacement ($\Delta_{v,n}$) can be computed by

$$\Delta_{v,n} = \gamma_n L \tag{A4}$$

where L is the length of the column and γ_n is the average shear strain at maximum shear strength which depends on the failure mode of the columns. For flexural-shear failure mode, this is given by

$$\gamma_n = \frac{1}{227370}\frac{f_y\sqrt{\rho}}{\left(\frac{a}{d}\right)\sqrt{\frac{P}{A_g f_c'}}} - 0.0006 \tag{A5}$$

For shear failure mode, the average shear strain at maximum shear strength is calculated by

$$\gamma_n = \frac{1}{172250}\frac{\left(\frac{a}{d}\right)f_{yt}\rho_{sh}}{\sqrt{\frac{P}{A_g f_c'}}} - 0.0011 \tag{A6}$$

In Eqs. (A5) and (A6), a is the shear span-length of the column, d is the member cross-section effective depth, f_{yt} are the yield strength of transverse reinforcements (MPa), and ρ and ρ_{sh} are the longitudinal and transverse reinforcement ratio, respectively. It should be noted that ρ and ρ_{sh} must be expressed in percentage.

Shear displacement ($\Delta_{v,u}$) of the column at the onset of shear strength degradation is determined by

$$\Delta_{v,u} = \left(4 - 12\frac{(V_n/bd)}{f_c'}\right)\gamma_n L \tag{A7}$$

Finally, for shear displacement at failure ($\Delta_{v,f}$), the equation proposed by Elwood and Moehle (2005) can be used

$$\Delta_{v,f} = \frac{4}{100}\frac{1+\tan^2\varphi}{\tan\varphi + P\left(\frac{s}{A_{sh} f_{yt} d_c \tan\varphi}\right)}L \tag{A8}$$

where b is the member cross-section width, A_{sh} is a transverse reinforcements area, φ is the expected shear crack angle (φ=65° as recommended by Elwood and Moehle 2005), d_c is the core-concrete depth which measures the center-to-center dimension of transverse reinforcement and s is transverse reinforcement spacing.

• Masonry infill panel properties

The maximum strength ($V_{\max}$) of the infill panel associated with corner-crushing and sliding-shear failure modes were considered as follow

For corner-crushing failure mode, the strength is calculated by

$$V_{cc} = wt_w f'_m \cos\theta \tag{A9}$$

where θ is the inclination angle of the diagonal strut from the horizontal direction, t_w is thickness of infill panel, f'_m is the masonry compressive strength, and w is the total effective width of the diagonal strut given by

$$w = 0.175(h\lambda)^{-0.4} d_w \tag{A10}$$

In the above equation, d_w is masonry panel diagonal length, h is story height, and λ is the relative stiffness between the surrounding frame and masonry infill panel (Smith and Carter 1969)

$$\lambda = \sqrt[4]{\frac{E_m t_w \sin 2\theta}{4EIh_w}} \tag{A11}$$

where E and E_m are moduli of elasticity of the surrounding frame and masonry infill panel, respectively, I is moment of inertia of the column, and h_w is infill panel height.

For sliding-shear failure mode, the lateral load resistance capacity, V_{slide}, is given by

$$V_{slide} = \frac{\tau_0 L_w t_w}{(1 - \mu\tan\theta)} \tag{A12}$$

where τ_0 is the cohesive capacity, μ is the friction coefficient, and L_w, t_w, and θ are related to the frame geometry. In this study, the lower-bound values for τ_0 and μ

were obtained by calibrating the strength with the lateral capacity of un-retrofitted (fully infilled) specimen tested by Srechai and Lukkunaprasit (2013), resulting in the cohesive capacity (τ_0) of 0.6 MPa and the friction coefficient (μ) of 0.74.

Finally, the contact length (Z) between the RC column and the infill panel can be expressed as a function of the relative stiffness (λ) as follows

$$Z = \frac{\pi}{2\lambda} \tag{A13}$$

Symbol list

The following symbols are used in this paper

A_g = gross-sectional area of column
A_{sh} = transverse reinforcement area
A_w = cross-sectional area of masonry panel
a = shear span length of the column
b = member cross-section width
d = member cross-section effective depth
d_c = core-concrete depth which measures the center-to-center dimension of transverse reinforcement
d_w = masonry panel diagonal length
E = modulus of elasticity of surrounding frame
E_m = modulus of elasticity of masonry panel
f_c' = compressive strength of concrete
f'_m = compressive strength of masonry
f_y = yield strength of longitudinal reinforcement
f_{yt} = yield strength of transverse reinforcements
G_w = shear modulus of masonry panel
h = story height
h_w = masonry panel height
I = moment of inertia of column
I_w = moment of inertia of masonry panel
K_c = softening stiffness of flexural plastic hinge
K_{fl} = flexural stiffness of a cantilever masonry panel
K_{ini} = initial stiffness of masonry panel
K_s = post-yielding stiffness of the column section
K_{sh} = shear stiffness of a cantilever masonry panel
K_{sof} = softening stiffness of masonry panel
L = length of the column
L_w = width of masonry panel
M_c = maximum moment
M_y = yielding moment
P = axial load
s = transverse reinforcement spacing
t_w = thickness of masonry panel
V_{cc} = lateral capacity of corner-crushing failure mode
V_{cr} = cracking shear strength
V_{max} = maximum strength of masonry panel
V_n = maximum shear strength of column
V_{res} = residual strength of masonry panel
V_{slide} = lateral capacity of sliding along the bed-joint failure mode
V_y =yield strength of masonry panel
w = total effective width of the diagonal struts
Z = contact length between columns and URM panel
Δ_{max} = lateral displacement of masonry panel at maximum strength
Δ_y = lateral displacement of masonry panel at yielding strength
Δ_{res} = lateral displacement of masonry panel at residual strength
$\Delta_{v,cr}$ = shear displacement at cracking strength
$\Delta_{v,f}$ = shear displacement at axial load failure
$\Delta_{v,n}$ = shear displacement at maximum strength
$\Delta_{v,u}$ = shear displacement at the onset of shear strength degradation
θ = inclination angle of the diagonal strut from the horizontal direction
θ_{pc} = post-capping rotation capacity of the column section
θ_{cap}^{pl} = plastic rotation capacity of the column section
λ = relative stiffness of the surrounding frame and masonry infill panel
γ_n = average shear strain at maximum shear strength of column
v = axial load ratio
μ = friction coefficient
ρ = total longitudinal reinforcement ratio
ρ_{sh} = transverse reinforcement ratio
τ_0 = cohesive capacity
φ = expected shear crack angle